Surface Science 651 (2016) 128–136

Contents lists available at ScienceDirect

Surface Science

journal homepage: www.elsevier.com/locate/susc

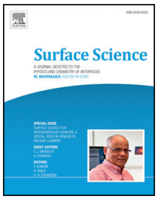

Effect of CaO on the selectivity of N_2O decomposition products: A combined experimental and DFT study

Lingnan Wu [a,b], Xiaoying Hu [b], Wu Qin [b], Pan Gao [b], Changqing Dong [b,*], Yongping Yang [a,*]

[a] School of Energy, Power and Mechanical Engineering, North China Electric Power University, Beijing 102206, China
[b] National Engineering Laboratory for Biomass Power Generation Equipment, North China Electric Power University, Beijing 102206, China

ARTICLE INFO

Article history:
Received 27 October 2015
Received in revised form 11 April 2016
Accepted 12 April 2016
Available online 16 April 2016

Keywords:
NO selectivity
Density functional theory
CaO (1 0 0)
N_2O decomposition

ABSTRACT

The effect of CaO on N_2O decomposition and the selectivity of its decomposition products (NO and N_2) was investigated using a fixed-bed flow reactor with varying temperatures from 317 °C to 947 °C. The selectivity of NO from CaO-catalyzed N_2O decomposition is much lower than the N_2 selectivity with the N_2/NO products ratio greater than 12.1. Compared to N_2O homogeneous decomposition with the minimum N_2/NO products ratio of 6.2 at 718 °C, CaO also decreases the NO selectivity from 718 °C to 947 °C. Density functional theory calculations provide possible N_2O decomposition routes on the CaO (1 0 0) surface considering both N_2 and NO as N_2O decomposition products. The N_2 formation route is more favorable than the NO formation route in terms of energy barrier and reaction energy, and NO formation on the CaO (1 0 0) surface is likely to proceed via $N_2O+O^{2-}_{surf}\rightarrow N_2+O^{2-}_{2,surf}$ and $N_2O+O^{2-}_{2,surf}\rightarrow 2NO+O^{2-}_{surf}$.

1. Introduction

Power generation from coal and biomass combustion is an important source of nitrogen oxides (NO_x) emissions. Compared to conventional pulverized coal-fired power plants, circulating fluidized bed (CFB) boilers have lower furnace temperatures, which is beneficial for reducing thermal NO_x formation. N_2O emission, however, soars to the range of 20–360 mg/Nm^3 [1,2], which is about ten times the amount of conventional pulverized coal-fired power plants. N_2O is a powerful greenhouse gas (310 times and 21 times greater than CO_2 and CH_4, respectively, in terms of global warming potential [3]) and it is speculated to be the most important ozone-depleting substance in the 21st century [4]. Therefore, the effective control of both NO_x and N_2O emissions is of equal importance for CFB boilers.

The in situ *de*SO_x process in the furnace of CFB boilers affects N_2O and NO_x emissions simultaneously. For atmospheric CFB boilers, the in situ *de*SO_x process proceeds via Reactions (1) and (2) [5] with the limestone calcined into calcium oxide (CaO), which acts as the SO_x sorbent in the furnace. CaO is therefore widely used to study the influence of limestone on in-furnace processes of CFB boilers.

$$CaCO_3\rightarrow CaO+CO_2 \quad \Delta H=182.1\ \mathrm{kJ/mol} \tag{1}$$

$$CaO+SO_2+\frac{1}{2}O_2\rightarrow CaSO_4 \quad \Delta H=-481.4\ \mathrm{kJ/mol} \tag{2}$$

The effect of limestone (or CaO) on the formation and decomposition of N_2O and NO has been extensively studied [6–17]. In general, limestone addition can increase NO emissions [7,8,10–13], but experimental results are controversial about the effect of CaO on N_2O emissions depending on the experimental scale. For full-scale experiments, Åmand et al. [7] found that limestone addition could reduce N_2O emission, while Bonn et al. [2] and Jensen et al. [10] found that there was little influence, or the influence depended on the furnace temperature [17]. For laboratory-scale experiments, it is widely agreed that CaO could reduce N_2O emissions by decreasing the selectivity of N_2O precursor (mainly HCN) to generate N_2O [9–12], or by catalyzing N_2O decomposition [15,16,18–22]. The attention of these studies has focused on the catalytic ability of CaO to affect the formation and decomposition of N_2O, or the overall emissions of N_2O and NO in large-scale experiments. To the best of our knowledge, however, how CaO affects the selectivity of N_2O decomposition products is not well studied.

Besides experimental studies, theoretical investigations using density functional theory (DFT) calculations have been performed to explain the catalytic effect of CaO for N_2O decomposition [20,23–29]. The CaO (1 0 0) surface was commonly used to study various CaO-involved processes [24–26,30–32] as it is the most stable low-index surface of CaO [33]. Previous studies have reported possible N_2O adsorption geometries on the CaO (1 0 0) surface [26,28,29], the O atom transfer from N_2O molecule to the surface [20,23,25,26,28], and the recovery of CaO (1 0 0) surface either by N_2O [23–25] or CO [27]. These studies outlined the mechanism of N_2O decomposition on the CaO surface and

---

* Corresponding authors.
E-mail addresses: wulingnan@126.com (L. Wu), huxy@ncepu.edu.cn (X. Hu), qinwugx@126.com (W. Qin), gaopan@ncepu.edu.cn (P. Gao), cqdong1@163.com (C. Dong), yypncepu@163.com (Y. Yang).

http://dx.doi.org/10.1016/j.susc.2016.04.004
0039-6028/

considered N_2 and O_2 as N_2O decomposition products, but how CaO affects NO formation from N_2O decomposition is still unclear. The mechanism of NO formation during the N_2O decomposition process is also important as both N_2O and NO emissions need to be strictly controlled.

To this end, we investigated the effect of CaO on NO formation and the selectivity of N_2O decomposition products using a fixed-bed flow reactor. Possible NO formation mechanisms from N_2O decomposition on the CaO (1 0 0) surface were explored using DFT calculations. Homogeneous and CaO-catalyzed NO formation routes and their competition with the N_2 formation route from N_2O decomposition was considered. The results are beneficial for a better understanding of the effect of CaO on N_2O decomposition and NO formation in CFB boilers, which will contribute to proposing synergetic NO–N_2O–SO_x control strategies.

2. Methodology

2.1. Experimental details

Fig. 1 shows the flowsheet of the laboratory-scale experimental apparatus. Flow rates of N_2O and balance gas (argon) were controlled by mass flowmeters and a total flow rate of 3000 mL/min at standard conditions was selected. An on-line FTIR analyzer (MB3000, ABB) was used to analyze tail-gas composition. NO, N_2O and NO_2 are IR active species with their IR spectrum shown in Fig. 2, and the concentrations of NO, N_2O and NO_2 can be correlated with the intensity of the absorbance spectrum. Measured values of standard NO, N_2O and NO_2 gases at specific concentration are shown in Fig. S1. A good correlation can be obtained when calibrating the measured concentrations of NO, N_2O and NO_2 against their known concentrations. In this way, the concentrations of NO, N_2O and NO_2 can be quantitatively obtained. However, N_2 and O_2 cannot be detected as they are not IR active. To the best of our knowledge, only N_2 and NO have been discussed as possible N_2O homogeneous decomposition products [34]. Besides, NO_2 is found to be negligible (always lower than 5 ppm) from N_2O decomposition in experiments. Therefore, the concentration of N_2 is calculated according to the measured conversion of N_2O and the concentration of NO formation.

The inlet N_2O concentration was fixed at 2000 ppm. A quartz reactor was used to study the effect of CaO on N_2O decomposition and the selectivity of decomposition products with 14 mm inner diameter and 600 mm heating length (heated by an electric furnace). The furnace temperature was monitored by a thermocouple mounted in the middle of the electric furnace and controlled by a PID temperature controller. The temperature of the reaction zone where the catalysts were placed was measured before performing experiments, and its correlation with the furnace temperature is shown in Fig. S2. A linear fitting between the furnace temperature and the reaction zone temperature was performed and the adjusted R^2 value of 0.9887 was obtained. In the following experiments, the effect of CaO on N_2O conversion, NO yield and NO selectivity was investigated with furnace temperature ranging from 300 °C to 950 °C with 100 °C temperature intervals. Corresponding reaction temperatures are 317 °C, 418 °C, 520 °C, 620 °C, 718 °C, 812 °C, 902 °C, and 947 °C respectively.

Analytically pure CaO (98%) was used in all experiments. A sheet of quartz wool was placed on the supporter for supporting CaO (for the blank group, only a sheet of quartz wool was placed). The particle diameter of CaO ranges from 0.18 to 0.25 mm. The CaO sample is characterized using Brunner–Emmet–Teller (BET), X-ray diffraction (XRD), scanning electron microscope (SEM), and X-ray fluorescence (XRF) methods. Obtained BET specific surface area of the CaO sample is 2.761 m^2/g, and the average pore diameter is 10.58 nm. From the XRD result shown in Fig. S3, it can be seen that CaO is well crystallized, and little amount of $Ca(OH)_2$ is detected as a result of the reaction between CaO and the H_2O in the air. The XRF result of the CaO sample is tabulated in Table S1 in metal oxide form. The loss on ignition value is 3.86%, which is speculated to be the contribution from H_2O captured by CaO in the air. The weight of CaO relative to the total weight detected by XRF analysis is calculated to be 98.88%. The morphology of the CaO sample characterized by SEM method is shown in Fig. S4. From XRD result (Fig. S3), only small amounts of $Ca(OH)_2$ species are detected except CaO. XRF result (Table S1) reports that the purity of CaO reaches as high as 98.88%. It can also be seen from the XRF results that the impurity of the CaO sample is composed of a mixture of 16 species rather than a single kind of species, of which Al_2O_3 and MgO are the two main impurities of the CaO sample with 0.55% and 0.38% weight ratio. Al_2O_3 is a well-known inert material for N_2O decomposition and often used as catalyst carrier [35]. MgO is more active than Al_2O_3 in decomposing N_2O but its activity is still lower than CaO [20]. Therefore, considering the

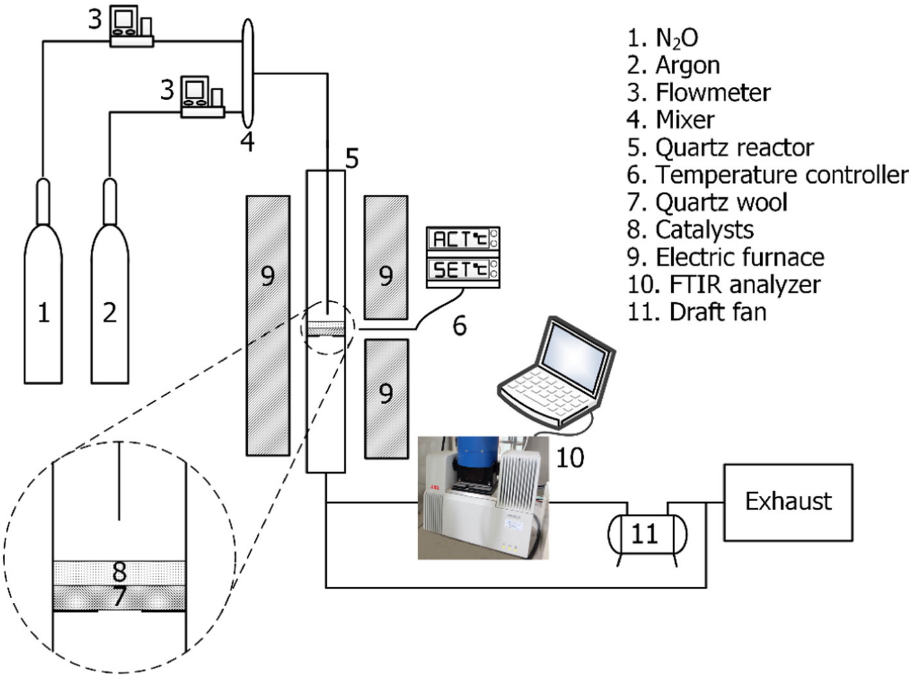

Fig. 1. Schematic of experimental apparatus.

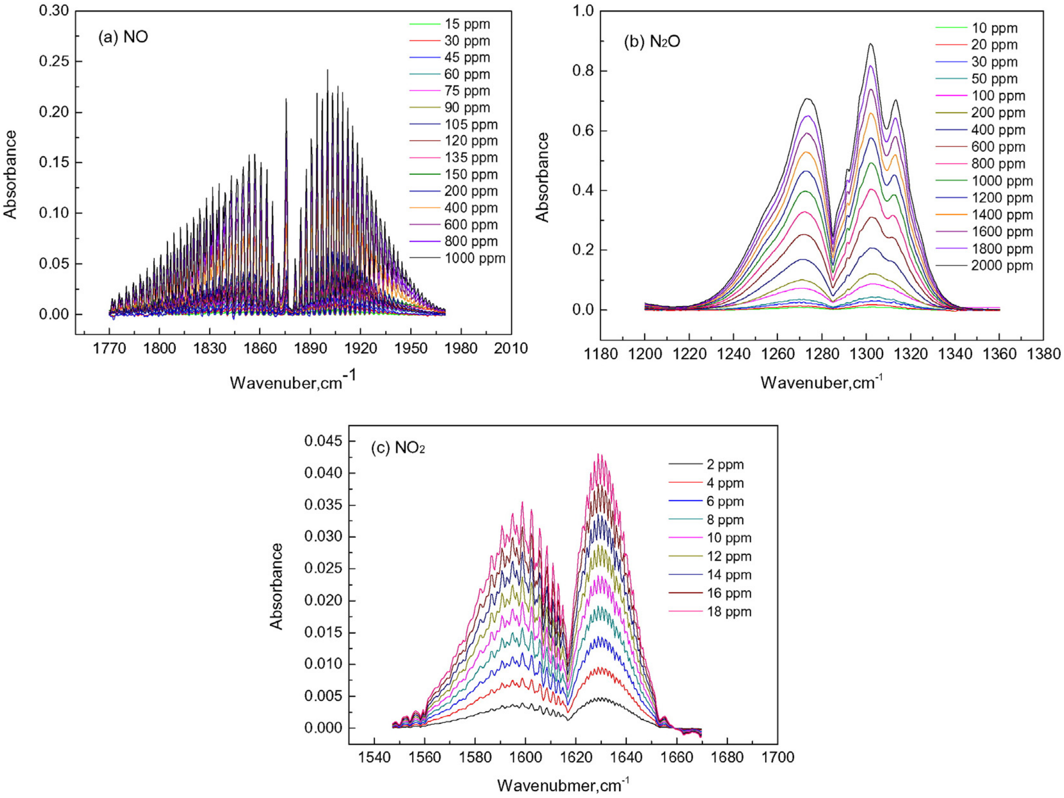

Fig. 2. Absorbance spectrometry of (a) NO; (b) N_2O; (c) NO_2.

amount and the activity of detected impurities, the observed experimental results of the decomposition and selectivity of N_2O are attributed to the effect of CaO rather than other species. To evaluate the effect of CaO on N_2O conversion, NO yield and NO selectivity, the N_2O conversion (X_{N_2O}) is defined as:

$$X_{N_2O} = \left(1 - \frac{n_{N_2O,out}}{n_{N_2O,in}}\right) \times 100\%$$

where $n_{N_2O,in}$ is the inlet N_2O concentration (ppm) of the reaction tube, and $n_{N_2O,out}$ is the outlet N_2O concentration (ppm) measured by the FTIR analyzer.

The NO yield (Y_{NO}) is defined as:

$$Y_{NO} = \frac{n_{NO,out}}{n_{N_2O,in}} \times 100\%$$

where $n_{NO,out}$ is the outlet NO concentration (ppm) after the reaction gas passes the catalyst layer.

The NO selectivity (S_{NO}) is defined as:

$$S_{NO} = \frac{n_{NO,out}}{n_{N_2O,in} - n_{N_2O,out}} \times 100\%$$

2.2. Computational details

DFT calculations were carried out using $DMol^3$ code [36,37] with generalized gradient approximation (GGA) and Perdew–Burke–Ernzerhof (PBE) functional [38] for exchange and correlation potentials. The atomic basis functions were expanded by double numerical basis sets plus polarization function (DNP). $DMol^3$ code with GGA and PBE functionals provided satisfactory calculation results with negligible basis set superposition error [39], which was comparable with the Gaussian 6–31G** basis set [25]. The BSSE error was tested using a periodic CaO surface slab model with a vacuum layer thickness of 92 Å. A N_2O molecule was placed 40 Å away from the CaO (1 0 0) surface, and the electronic energies of the CaO (1 0 0) surface with N_2O molecule, pure CaO (1 0 0) surface and N_2O molecule were calculated. Results showed that the absolute value of BSSE error was only 0.002 eV, which was very trivial compared to the energy profiles in this study.

CaO belongs to the cubic crystal system with *Fm3m* (225) space group numbering. The lattice constant was 4.854 Å (4.883 Å [30] and 4.840 Å [33]) after geometric optimization. The CaO (1 0 0) surface was used as it was the most stable low-index facet of CaO [33]. To establish the CaO (1 0 0) surface, a five-layer CaO (1 0 0) slab was cleaved from a perfect CaO crystal with the top two layers fully relaxed and bottom three layers frozen. A sheet of 12 Å vacuum layer was built above the slab surface to eliminate the interference from imaging layers. The surface was expanded with a 2 × 2 supercell containing 80 cations and anions (40 Ca cations and 40 O anions) (Fig. 3). A 3 × 3 × 1 Monkhorst–Pack *k*-point sampling grid was used for Brillouin zone integration during geometric, energetic and transition state search calculations. Atomic radius orbital cut-off was selected as 4.8 Å. 0.005 Ha Fermi smearing was selected for convergence acceleration. A combination of linear synchronous transit (LST) and quadratic synchronous transit (QST) methods [40] were employed to search the transition state of reactions. The transition state was then further optimized with eigenvector following (EF) method to guarantee only one imaginary frequency exists.

To evaluate the interaction between the adsorbate and the CaO (1 0 0) surface, the adsorption energy (E_{ad}) is defined as:

$$E_{ad} = E_{sys} - E_{ads} - E_{sur}$$

where E_{sys} is the system total energy after adsorption, E_{ads} is the energy of adsorbate, and E_{sur} is the energy of the surface before adsorption.

To consider the influence of temperature on the elementary reaction steps, free Gibbs energy is calculated, which considers the zero point

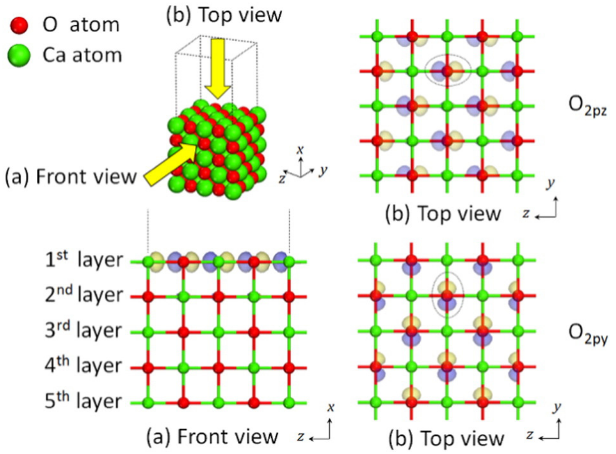

Fig. 3. Structure of CaO (1 0 0) surface.

energy and the thermal contributions to the electronic energy from DFT calculations obtained from vibrational analysis. The frequency analysis is performed on the periodic surface slab. The translational and rotational movements of surface adsorbed species are incorporated in vibrational analysis, and the vibrations of the atoms in the model are based on the harmonic oscillator approximation. The harmonic oscillator approximation method, however, suffers from an underestimation of the entropies of surface adsorbed species [41]. Based on vibrational analysis results, enthalpy and entropy at different temperatures can be calculated, and the Gibbs free energy can be obtained. The activation Gibbs free energy G_a is the Gibbs free energy difference between the transition state (G_{TS}) and the reactant state (G_{IS}), which is:

$$G_a = G_{TS} - G_{IS}.$$

The Gibbs free reaction energy ΔG is the Gibbs free energy difference between the product state (G_{FS}) and the reactant state (G_{IS}), which is:

$$\Delta G = G_{FS} - G_{IS}.$$

3. Results and discussion

3.1. Experimental results

The effect of CaO on N_2O conversion is illustrated in Fig. 4a. For the blank group, N_2O conversion is only 1.3% at 620 °C, and it increases with the increase of reaction zone temperature, which is 5.0%, 30.8%, 80.4% and 94.5% at 718 °C, 812 °C, 902 °C and 947 °C. Although no catalyst is placed in the reaction zone, the N_2O conversion even reaches 94.5%. at 947 °C, which agrees with the unstable thermodynamic properties of N_2O. The addition of CaO greatly enhances the N_2O conversion for the temperature range from 620 °C to 947 °C. At 620 °C, X_{N_2O} reaches 65.0%, and it increases sharply to 99.5% at 718 °C. From 718 °C to 947 °C the X_{N_2O} remains higher than 99.5%. Therefore, it is clear that CaO shows strong catalytic ability for N_2O decomposition in comparison to N_2O homogeneous decomposition. This result is consistent with previous experimental studies of Hansen et al. [15] using a laboratory-scale fixed-bed quartz reactor in the temperature range from 800 °C to 950 °C, Snis et al. [20] using a fixed-bed quartz reactor in the temperature range from 500 °C to 950 °C, and Piskorz et al. [25] using a fixed-bed microreactor from 400 °C to 650 °C.

The effect of CaO on NO yield from N_2O decomposition is shown in Fig. 4b. For the blank group and CaO-catalyzed N_2O decomposition group, NO is not formed from N_2O decomposition when the reaction zone temperature is lower than 620 °C. When the temperature of the reaction zone is higher than 620 °C, the NO yield begins to increase. There is almost no difference for NO yield between the blank group and the CaO group below 812 °C, but when temperature reaches 902 °C and 947 °C, the NO yield of the blank group is 1.5% and 1.7% higher than the CaO group. Therefore, the addition of CaO could slightly reduce the

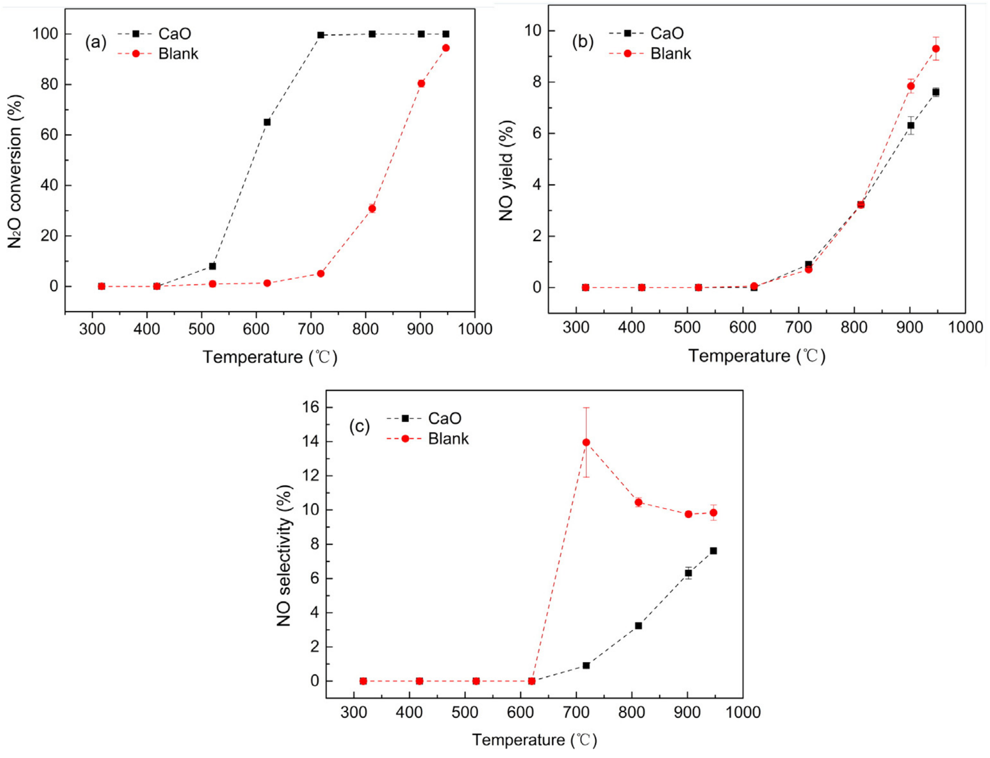

Fig. 4. The effect of CaO on (a) N_2O conversion; (b) NO yield and; and (c) NO selectivity.

NO yield from N_2O decomposition when temperature is between 812 °C and 947 °C.

The effect of CaO on NO selectivity during the N_2O decomposition process is shown in Fig. 4c. The NO selectivity below 620 °C is insignificant as NO will not be formed from N_2O decomposition when temperature is lower than 620 °C. When the reaction zone temperature reaches 718 °C, a significant increase of NO selectivity is seen for the blank group. This increase for the blank group can be attributed to the low conversion of N_2O and the increase of NO formation at 718 °C (around 14.0%). Its error range is around 4% due to the fact that the absolute conversion of N_2O at 718 °C is so low that the small relative increase of the NO product is prominently observable in the NO fraction. In comparison to the catalyzed sample, this is correct, as the total conversion is much larger at this temperature for the catalyzed process leading to N_2 rather than NO. The absolute conversion increases to 5% with about 1% NO, leading to a selectivity of NO (out of all products) of about 20%. In Fig. 4c, this is about 14% with a 5% error, and that matches well enough. When reaction temperature further increases from 718 °C, a decreasing trend for the blank group and an increasing trend for the CaO group is seen, and the NO selectivity of the blank group is 7.2%, 3.4% and 2.2% higher, respectively, than that of the CaO group. Therefore, the presence of CaO is able to reduce the NO selectivity from N_2O decomposition from 718 °C to 947 °C. For the CaO catalyzed N_2O decomposition, the N_2/NO products ratio decreases with the increase of temperature. Its value is 109.7 at 718 °C, 19.9 at 812 °C, 14.8 at 902 °C and the N_2/NO products ratio reaches the lowest value of 12.1 at 947 °C. For the homogeneous N_2O decomposition, the N_2/NO value reaches its lowest value of 6.2 at 718 °C, and it gradually increases to 8.6 at 812 °C, reaches a peak of 9.3 at 902 °C and decreases to 9.2 at 947 °C.

Argon is used as the balance gas instead of N_2 to avoid interference between the diluent and generated O_2. The generated N_2 from N_2O decomposition, however may also react with the generated O_2 following the Zeldovich mechanism through $N_2+O \rightarrow NO+N$ and $O_2+N \rightarrow NO+O$ [42]. This reaction is not considered in the following discussion as thermal formation of NO is not significant until temperature exceeds 1800 K (1527 °C) [43], which is beyond the temperature range (below 947 °C) of this study. Furthermore, when using a N_2 and O_2 mixture as the inlet gas (with 2:1 M ratio) from room temperature to 947 °C, NO was not detected. This is consistent with the Zeldovich mechanism [42] and rules out the NO formation route from homogeneous reaction between N_2 and O_2.

To investigate the effect of CaO on NO formation during the N_2O catalytic decomposition process, the mechanism of NO formation on the CaO (1 0 0) surface is studied in the following sections based on density functional theory calculations.

3.2. Homogeneous decomposition of N_2O

The mechanism of N_2O homogeneous decomposition is first investigated for comparison purposes. Two kinds of N-containing products generated from N_2O decomposition are considered, N_2 and NO, as formulated in Reactions (3) and (4):

$$2N_2O \rightarrow 2N_2 + O_2 \tag{3}$$

$$2N_2O \rightarrow 2NO + N_2 \tag{4}$$

The elementary reactions of N_2O decomposition into N_2 and O_2 following Reaction (3) are:

$$N_2O \rightarrow N_2 + O \tag{5}$$

$$N_2O + O \rightarrow N_2 + O_2 \tag{6}$$

The generated O radical can also react with a second N_2O forming two NO molecules following Reaction (7):

$$N_2O + O \rightarrow NO + NO \tag{7}$$

Reactions (5) to (7) consider the N–O bond cleavage during N_2O homogeneous decomposition. The possibility of N–N bond cleavage and its succeeding reaction with N_2O are also discussed according to Reactions (8) and (9):

$$N_2O \rightarrow NO + N \tag{8}$$

$$N_2O + N \rightarrow NO + N_2 \tag{9}$$

Fig. 5 provides the energy profiles and the geometries of Reactions (5) to (9). The homogeneous N–O bond cleavage of N_2O needs 2.926 eV to generate an O radical and a N_2 molecule, while the generation of a N radical and NO is much more demanding with 5.768 eV needed (Fig. 5a).

Then the generated O radical can attack both the O end and the N end of a second N_2O molecule following Reactions (6) and (7) as shown in Fig. 5b. The generation of N_2 and O_2 needs to pass the energy barrier of 1.017 eV. By comparison, the reaction between O radical and N_2O only needs to overcome a 0.400 eV energy barrier and generates an ONNO complex. The generated ONNO complex needs additional 0.476 eV to detach into two NO molecules, which is the rate determining step for NO formation. Another possibility of NO formation is shown in Fig. 5c, which is caused by the reaction of N radical with a second N_2O molecule, with the energy barrier of 1.305 eV. Comparing the above possible routes, N_2O decomposition is determined by the bond cleavage step, and the cleavage of the N–O bond is more likely than the N–N bond as a matter of lower energy barrier. For this section, the energy profile of N_2O homogeneous decomposition is provided for comparison with CaO-catalyzed N_2O decomposition. Further details of higher quality calculations on N_2O homogeneous reaction with O (^3P) based on ab initio CASPT2//CASSCF methods can be referenced elsewhere [34].

3.3. Mechanism of N_2O decomposition into N_2 and O_2 on the CaO (1 0 0) surface

The mechanism of N_2O decomposition into N_2 and O_2 on the CaO (1 0 0) surface is investigated and summarized in Fig. 6 for comparison with NO formation routes. N_2O decomposition into N_2 and O_2 on the CaO (1 0 0) surface initiates from the O atom transfer from a N_2O molecule to the surface O anion site, forming surface peroxy species with a 0.989 eV energy barrier, which is much lower than that of homogeneous N_2O decomposition (2.926 eV). The effect of exchange and correlation functionals on the energy barrier of O atom transfer step is listed in Table S2 in supplementary materials. It is found that GGA + PW91, GGA + BP, GGA + BOP, GGA + VWNBP, and LDA + VWN give similar results compared to the GGA + PBE functional, while GGA + BLYP and LDA + PWC gives relatively lower energy barriers and GGA + HCTH gives a much higher energy barrier.

Surface recovery needs to be taken into account at high surface coverage as the atomic O from N_2O decomposition poisons the active surface O anion. The surface adsorbed atomic O from N_2O decomposition can be removed following the Eley–Rideal (ER) mechanism by reacting with a second N_2O (Fig. 6a) or the Langmuir–Hinshelwood (LH) mechanism by recombination with a neighboring adsorbed atomic O (Fig. 6b). The calculated energy barriers of the ER and LH mechanisms are 1.200 eV and 1.400 eV respectively, and both of them are higher than that of the O atom transfer process. Therefore, whether under high or low surface coverage conditions, the energy barrier of N_2O decomposition on the CaO (1 0 0) surface is much lower than the

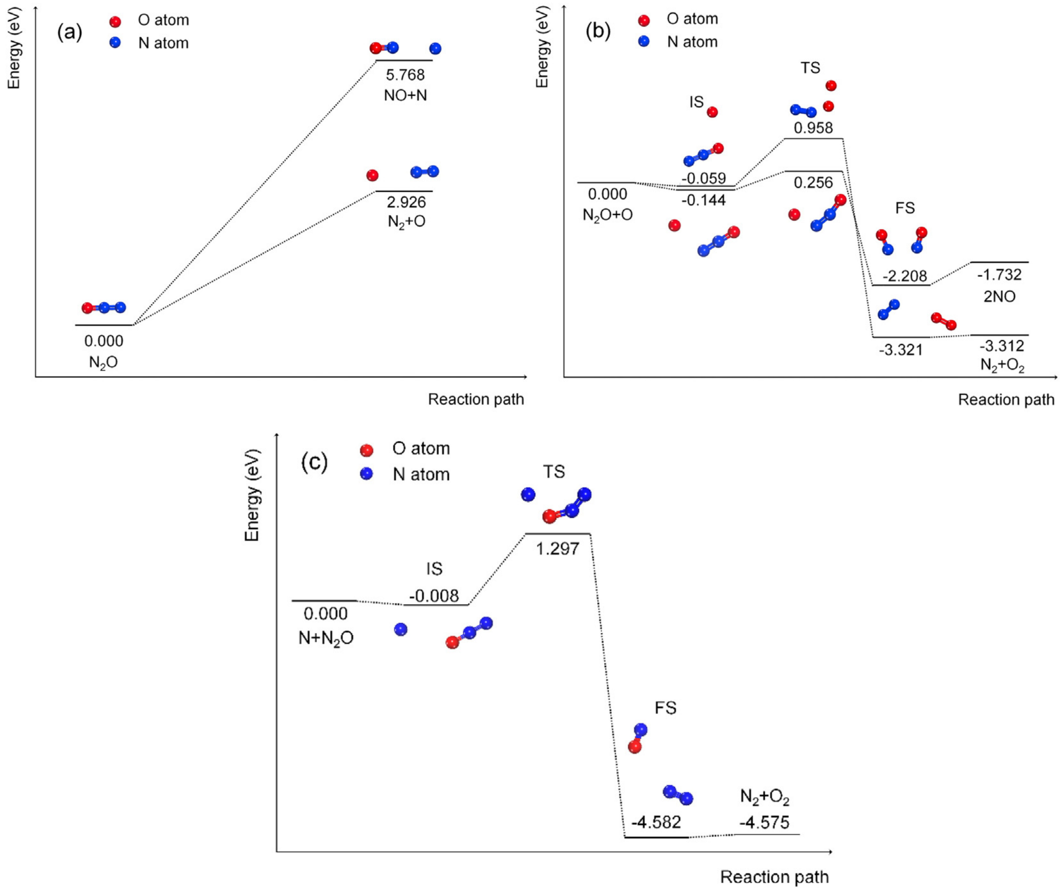

Fig. 5. Energy profile of N_2O homogeneous decomposition: (a) N–O and N–N bond cleavage; (b) reaction between O radical and a second N_2O; (c) reaction between N radical with a second N_2O.

homogeneous case, and CaO is therefore able to catalyze N_2O decomposition, which explains the experimental observations.

3.4. Mechanism of N_2O decomposition into NO and N_2 on the CaO (1 0 0) surface

In analogy with the NO homogeneous formation mechanism, two NO formation routes from N_2O decomposition on the CaO (1 0 0) surface are considered, depending on the order of bond cleavage (the N–O bond cleavage first and N–N bond cleavage first). The CaO (1 0 0) surface could catalyze the N–O bond cleavage of N_2O according to Reaction (10) (the O atom transfer step) or the N–N bond cleavage according to Reaction (11):

$$N_2O + O^{2-}_{surf} \rightarrow N_2 + O^{2-}_{2,surf} \tag{10}$$

$$N_2O + O^{2-}_{surf} \rightarrow NO + N - O^{2-}_{surf} \tag{11}$$

where O^{2-}_{surf} is the unsaturated five-fold O anion site on the CaO (1 0 0) surface.

The energy profiles of the N–O and N–N bond cleavage catalyzed by the CaO (1 0 0) surface are shown in Fig. 7. The cleavage of the N–O bond of N_2O is greatly facilitated by the energy barrier decrease from 2.926 eV to 0.989 eV as mentioned previously. For the N–N bond cleavage on the CaO (1 0 0) surface, an energy barrier of 1.412 eV is needed for the N_2O molecule to chemisorb with a bent NNO structure on the surface O anion site. The chemisorption process needs to adsorb 0.671 eV, and further N–N bond cleavage needs 3.312 eV to generate a NO molecule and a surface adsorbed atomic N. Although the CaO surface catalyzes the N–N bond cleavage of N_2O, this route is still very energy intensive in order to proceed.

Partial density of states (PODS) analysis is performed to investigate the electronic properties of the adsorbed atomic O and N on the surface O anion site (Fig. 8). The 2*s* and 2*p* orbitals of the O atom of N_2O and the surface O anion are located at different energy levels, which is consistent with the weak interaction between the surface and the N_2O molecule before the O atom transfer process. When the O atom of N_2O is transferred to the surface O anion site, a good match between the electronic states of the adsorbed atomic O and the surface O anion is seen at −21.1 eV, −19.2 eV and −14.1 eV (2*s* orbital) and −5.0 eV, −4.1 eV and −0.2 eV (2*p* orbital). A covalent bond is formed between the adsorbed atomic O and the surface O anion after the O atom transfer process. Similarly, the electron states of the N atom of N_2O and the surface O anion are located in different energy levels before N atom transfer from the N_2O molecule to the surface O anion. When N_2O reaches the chemisorption state, the electrons of the N atom overlaps the surface O anion in a much more delocalized range from −4.8 eV to Fermi level (2*p* orbital). With the cleavage of the N–N bond of the chemisorbed N_2O, the electron states of the adsorbed N atom and the O anion are still in good match but in a more localized area with the peaks at −5.6 eV and Fermi level (2*p* orbital), indicating a covalent bond is formed between the adsorbed N and the surface O anion.

The activity of the adsorbed atomic N and O on the CaO (1 0 0) surface O anion site for NO generation is then investigated by studying its reaction with a second N_2O molecule (Fig. 9). Reactions between the N_2O molecule and the surface adsorbed atomic O and N proceeds following Reactions (12) and (13):

$$N_2O + O^{2-}_{2,surf} \rightarrow 2NO + O^{2-}_{surf} \tag{12}$$

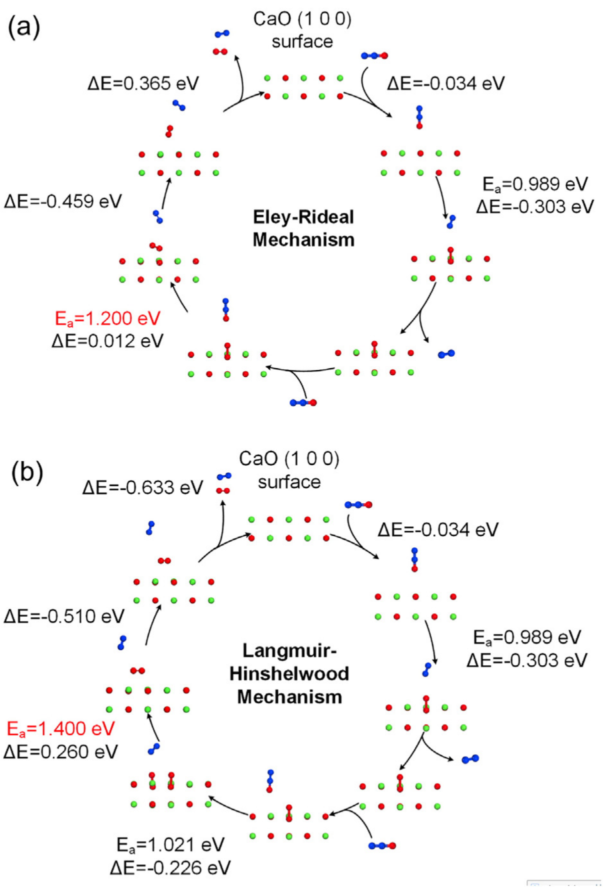

Fig. 6. N_2O decomposition routes on the CaO (1 0 0) surface: (a) following Eley–Rideal mechanism; (b) following Langmuir–Hinshelwood mechanism.

$$N_2O + N - O^{2-}_{surf} \rightarrow NO + N_2 + O^{2-}_{surf} \tag{13}$$

The energy profiles of Reactions (12) and (13) are illustrated in Fig. 9, and the upper part shows the reaction route between surface adsorbed atomic O with a second N_2O forming two NO molecules. The N_2O molecule will first overcome an energy barrier of 1.043 eV to attack the adsorbed atomic O forming an ONNO species with its N end adsorbed on the surface, which further needs 1.645 eV to desorb from the CaO surface and detach into two free NO molecules. The lower route of Fig. 9 is the reaction between a second N_2O with surface adsorbed atomic N, which needs to pass an energy barrier of 0.616 to form a surface adsorbed NO molecule and a N_2 molecule, with 2.940 eV heat release. The adsorbed NO molecule needs 0.612 eV to desorb from the CaO (1 0 0) surface. It is clear that the surface adsorbed N is more active than the surface adsorbed atomic O, but the formation of atomic N is much harder than that of atomic O with energy barriers of 3.983 eV and 0.989 eV respectively. Therefore, the NO formation from N_2O decomposition is more likely to proceed with an O atom transfer process first ($N_2O + O^{2-}_{surf} \rightarrow N_2 + O^{2-}_{2,surf}$) followed by a subsequent

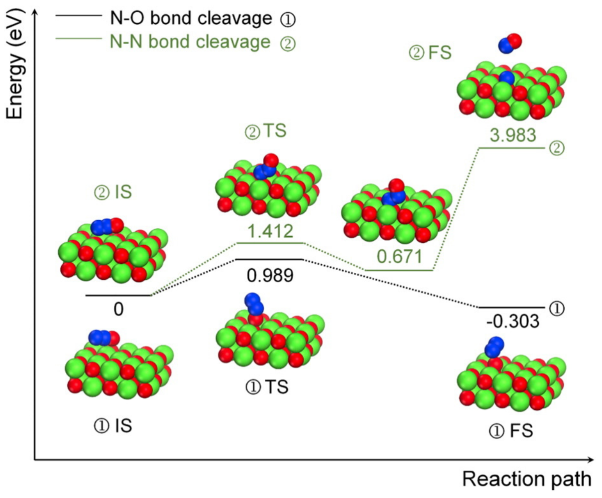

Fig. 7. Energy profiles of N–O and N–N bond breakage of N_2O on the CaO (1 0 0) surface.

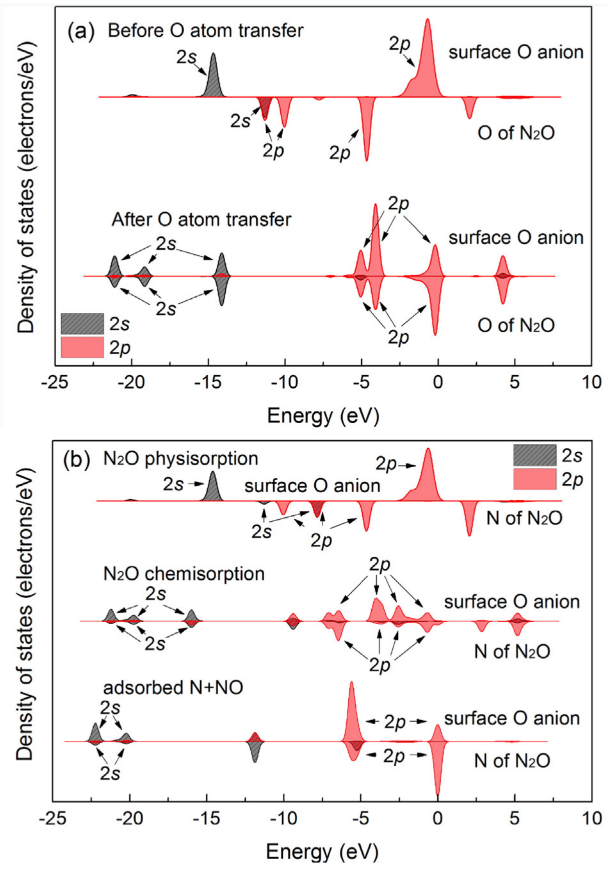

Fig. 8. PDOS analysis of the adsorbed atomic O and N before and after N_2O decomposition.

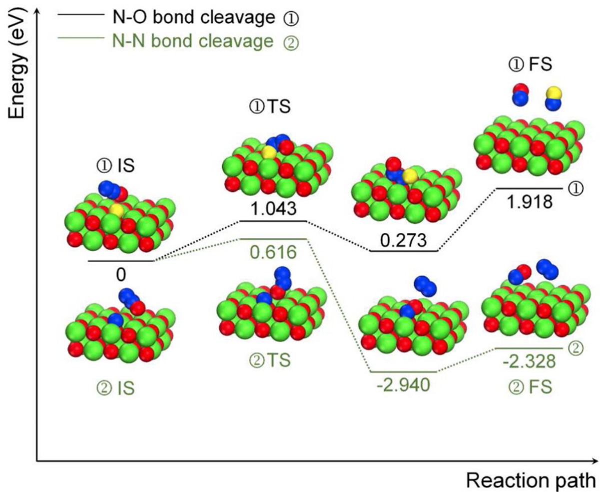

Fig. 9. NO formation from the reaction between surface adsorbed atomic O and N with a second N_2O molecule (the surface adsorbed O is highlighted for clarity).

reaction between the adsorbed atomic O and the N_2O molecule forming two NO molecules ($N_2O + O^{2-}_{2,surf} \rightarrow 2NO + O^{2-}_{surf}$), which needs to pass an overall energy barrier of 1.918 eV.

3.5. Temperature dependence of elementary reaction steps

As the above analysis only considers the electronic energy of respective reaction processes, the influence of temperature on each respective reaction step is investigated in this part to incorporate the thermal contributions to the elementary reaction steps. Fig. 10a shows the influence of temperature on the energy barrier of N_2O decomposition on the CaO (1 0 0) surface with initial N–O bond cleavage. The black line in Fig. 10a depicts the temperature influence on O atom transfer from N_2O to the surface O anion. A decreasing trend is observed with increasing temperature for the calculated temperature range. The red lines in Fig. 10a show the energy barrier change of surface recovery processes (following the ER and LH routes). Similarly, both of them show a decreasing trend with the increase of temperature. O atom transfer and ER or LH surface recovery processes are succeeding reaction steps for N_2O decomposition into N_2 and O_2. The energy barrier of the O atom transfer step is lower than the ER and LH surface recovery, indicating that N_2O decomposition into N_2 and O_2 is determined by the surface recovery process. The blue lines of Fig. 10a depict the influence of temperature on NO formation routes from adsorbed atomic O on the surface O anion reacting with a following N_2O molecule. The energy barrier of N_2O reacting with the adsorbed atomic O decreases with the increase of temperature, which forms surface adsorbed ONNO species, and its energy barrier is lower than the LH and ER surface recovery routes. The energy need for cleaving the formed ONNO into two NO molecules first decreases and then increases with the increase of temperature, which is higher than the LH and ER surface recovery routes and determines the rate for NO formation. Another NO formation route from N_2O decomposition on the CaO (1 0 0) surface with initial N–N bond cleavage is illustrated in Fig. 10b. The energy barrier for N_2O to form a surface adsorbed bent NNO species decreases with the increase of temperature. The bent NNO species on the CaO (1 0 0) surface needs formidable energy to break its N–N bond and forms NO and a surface adsorbed atomic N, making this NO formation route less likely than the other reaction route. Fig. 10c is the effect of temperature on the reaction energy of the same reaction steps as in Fig. 10a. For O atom transfer, ER, and LH surface recovery processes, the reaction energy is always negative for the considered temperature range, indicating that N_2O can decompose spontaneously on the CaO (1 0 0) surface. However, the reaction energy of adsorbed atomic O reacting with a following N_2O into ONNO is always positive, indicating that it cannot proceed spontaneously. The reaction energy of N_2O reacting with the CaO (1 0 0) surface into the bent NNO species is also greater than zero for the calculated temperature in Fig. 10d, and this process cannot proceed spontaneously for the calculated temperature range.

In terms of the above calculated activation Gibbs free energy and Gibbs free reaction energy, N_2O decomposition on the CaO (1 0 0) surface is more likely to generate N_2 and O_2 following O atom transfer and LH surface recovery process, while NO formation is comparatively less likely to be generated from N_2O decomposition. This can be attributed to the higher energy barrier of NO formation routes compared to N_2 formation routes, and the fact that NO formation routes cannot proceed spontaneously. Therefore, N_2 has a higher selectivity than NO when N_2O decomposes on the CaO (1 0 0) surface and the calculated results are consistent with our experimental observations. Meanwhile, for the homogeneous case, calculated results show that the generated O radical is more likely to react with a secondary N_2O forming NO rather than forming N_2 (which is offset by the O radical recombination reaction). The calculated selectivity for N_2 is higher than NO on the CaO (1 0 0) surface, so the selectivity of NO formation from N_2O decomposition is higher when CaO is present compared to N_2O homogeneous decomposition, which is in agreement with the experimental observations that CaO decreases the selectivity of NO from N_2O decomposition compared to the N_2O homogeneous decomposition.

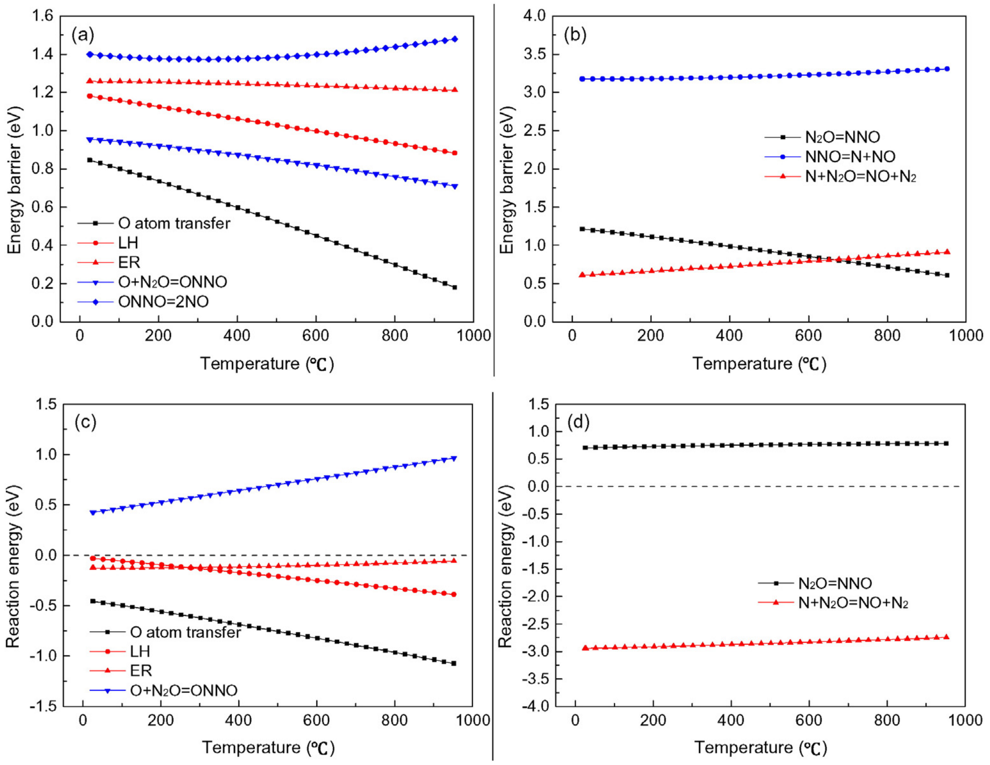

Fig. 10. Effect of temperature on the (a) energy barrier of elementary reaction steps with N–O bond cleavage at first; (b) energy barrier of elementary reaction steps with N–N bond cleavage at first; (c) reaction energy of elementary reaction steps with N–O bond cleavage at first; (d) reaction energy of elementary reaction steps with N–O bond cleavage at first.

4. Conclusions

Our experiments investigated the effect of CaO on N_2O decomposition and the selectivity of its decomposition products. Results show that CaO can catalyze N_2O decomposition compared to the homogeneous case, and N_2 has a higher selectivity than NO. Meanwhile, CaO decreases the NO selectivity compared to the homogeneous case. The N_2/NO products ratio of N_2O homogeneous decomposition reaches the minimum of 6.2 at 718 °C, while the N_2/NO products ratio of CaO catalyzed N_2O decomposition reaches its minimum of 12.1 at 947 °C. Density functional calculations were used to investigate the N_2 and NO formation routes from N_2O decomposition on the CaO (1 0 0) surface. Two NO formation routes were proposed and compared to N_2 and O_2 formation routes from N_2O decomposition both homogenously and heterogeneously on the CaO (1 0 0) surface. N_2 formation from N_2O decomposition is more likely than the NO formation route as a result of the relatively lower energy barrier and lack of spontaneous NO formation route. NO formation on the CaO (1 0 0) surface is more likely to proceed via $N_2O + O^{2-}_{surf} \rightarrow N_2 + O^{2-}_{2,surf}$ and $N_2O + O^{2-}_{2,surf} \rightarrow 2NO + O^{2-}_{surf}$.

Acknowledgments

The authors are grateful for the support of the National Natural Science Foundation of China (Grant No. 51206045), the Major State Basic Research Development Program of China (973 Program) (Grant No. 2015CB251501), 111 Project (Grant No. B12034), and the Fundamental Research Funds for the Central Universities (Grant No. 2015ZZD02). Special thanks to Aric Rousso from Princeton University for grammatical revisions to this paper.

Appendix A. Supplementary data

Supplementary data to this article can be found online at http://dx.doi.org/10.1016/j.susc.2016.04.004.

References

[1] M.A. Wójtowicz, J.R. Pels, J.A. Moulijn, Fuel Process. Technol. 34 (1993) 1.
[2] B. Bonn, G. Pelz, H. Baumann, Fuel 74 (1995) 165.
[3] United States Environmental Protection Agency, Overview of GreenhouseGases, (in) http://epa.gov/climatechange/ghgemissions/gases/n2o.html.
[4] A.R. Ravishankara, J.S. Daniel, R.W. Portmann, Science 326 (2009) 123.
[5] E.J. Anthony, D.L. Granatstein, Prog. Energy Combust. Sci. 27 (2001) 215.
[6] J.E. Johnsson, Fuel 73 (1994) 1398.
[7] L.-E. Åmand, B. Leckner, K. Dam-Johansen, Fuel 72 (1993) 557.
[8] K. Dam-Johansen, L.-E. Åmand, B. Leckner, Fuel 72 (1993) 565.
[9] A.N. Hayhurst, A.D. Lawrence, Combust. Flame 105 (1996) 511.
[10] A. Jensen, J.E. Johnsson, K. Dam-Johansen, Symp. Combust. 26 (1996) 3335.
[11] W. Lin, J.E. Johnsson, K. Dam-Johansen, C.M. van den Bleek, Fuel 73 (1994) 1202.
[12] T. Shimizu, Y. Tachiyama, D. Fujita, K. Kumazawa, O. Wakayama, K. Ishizu, S. Kobayashi, S. Shikada, M. Inagaki, Energy Fuel 6 (1992) 753.
[13] T. Shimizu, Y. Tachiyama, A. Kuroda, M. Inagaki, Fuel 71 (1992) 841.
[14] L.A.C. Tarelho, M.A.A. Matos, F.J.M.A. Pereira, Fuel 85 (2006) 967.
[15] P.F.B. Hansen, K. Dam-Johansen, J.E. Johnsson, T. Hulgaard, Chem. Eng. Sci. 47 (1992) 2419.
[16] B. Shen, T. Mi, D. Liu, B. Feng, Q. Yao, F. Winter, Fuel Process. Technol. 84 (2003) 13.
[17] A. Lyngfelt, B. Leckner, Fuel 72 (1993) 1553.
[18] V. Barišić, A.K. Neyestanaki, F. Klingstedt, P. Kilpinen, K. Eränen, M. Hupa, Energy Fuel 18 (2004) 1909.
[19] V. Barišić, F. Klingstedt, A. Naydenov, P. Stefanov, P. Kilpinen, M. Hupa, Catal. Today 100 (2005) 337.
[20] A. Snis, H. Miettinen, J. Phys. Chem. B 102 (1998) 2555.
[21] X. Hou, H. Zhang, S. Yang, J. Lu, G. Yue, Chem. Eng. J. 140 (2008) 43.
[22] D. Shun, H.S. Chang, Y.S. Park, D.H. Bae, G.T. Jin, Korean J. Chem. Eng. 18 (2001) 630.
[23] E.J. Karlsen, M.A. Nygren, L.G.M. Pettersson, J. Phys. Chem. A 106 (2002) 7868.
[24] A. Snis, I. Panas, J. Chem. Phys. 103 (1995) 7626.
[25] W. Piskorz, F. Zasada, P. Stelmachowski, A. Kotarba, Z. Sojka, J. Phys. Chem. C 117 (2013) 18488.
[26] L.N. Kantorovich, M.J. Gillan, Surf. Sci. 376 (1997) 169.
[27] A. Snis, I. Panas, D. Strömberg, Surf. Sci. 310 (1994) L579.
[28] A. Snis, D. Strömberg, I. Panas, Surf. Sci. 292 (1993) 317.
[29] L. Wu, W. Qin, X. Hu, C. Dong, Y. Yang, Appl. Surf. Sci. 333 (2015) 194.
[30] S. Zhang, X. Hu, Q. Lu, J. Zhang, Energy Fuel 25 (2011) 2932.
[31] L. Wang, Appl. Surf. Sci. 257 (2011) 5499.
[32] D. Strömberg, Surf. Sci. 275 (1992) 473.
[33] P. Broqvist, H. Grönbeck, I. Panas, Surf. Sci. 554 (2004) 262.
[34] M. González, R. Valero, R. Sayos, J. Chem. Phys. 115 (2001) 2540.
[35] K. Doi, Y.Y. Wu, R. Takeda, A. Matsunami, N. Arai, T. Tagawa, S. Goto, Appl. Catal. B Environ. 35 (2001) 43.
[36] B. Delley, J. Chem. Phys. 92 (1990) 508.
[37] B. Delley, J. Chem. Phys. 113 (2000) 7756.
[38] J.P. Perdew, K. Burke, M. Ernzerhof, Phys. Rev. Lett. 77 (1996) 3865.
[39] Y. Inada, H. Orita, J. Comput. Chem. 29 (2008) 225.
[40] N. Govind, M. Petersen, G. Fitzgerald, D. King-Smith, J. Andzelm, Comput. Mater. Sci. 28 (2003) 250.
[41] C.T. Campbell, J.R.V. Sellers, J. Am. Chem. Soc. 134 (2012) 18109.
[42] Y.B. Zeldovich, Acta Physicochim. URSS 21 (1946) 577.
[43] P. Glarborg, A.D. Jensen, J.E. Johnsson, Prog. Energy Combust. Sci. 29 (2003) 89.